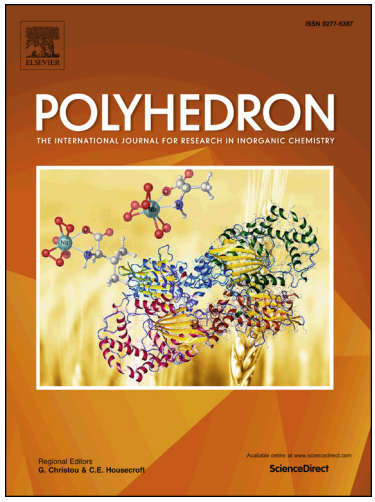

Synthesis, X-ray Structure, DFT Calculations and Anticancer Activity of a Selenourea Coordinated Gold(I)-Carbene Complex

Adam A.A. Seliman, Mohammad Altaf, Nurudeen A. Odewunmi, Abdel-Nasser Kawde, Wiktor Zierkiewicz, Saeed Ahmad, Saleh Altuwaijri, Anvarhusein A. Isab

PII: S0277-5387(17)30522-3
DOI: http://dx.doi.org/10.1016/j.poly.2017.08.003
Reference: POLY 12767

To appear in: *Polyhedron*

Received Date: 20 May 2017
Accepted Date: 2 August 2017

Please cite this article as: A.A.A. Seliman, M. Altaf, N.A. Odewunmi, A-N. Kawde, W. Zierkiewicz, S. Ahmad, S. Altuwaijri, A.A. Isab, Synthesis, X-ray Structure, DFT Calculations and Anticancer Activity of a Selenourea Coordinated Gold(I)-Carbene Complex, *Polyhedron* (2017), doi: http://dx.doi.org/10.1016/j.poly.2017.08.003

Synthesis, X-ray Structure, DFT Calculations and Anticancer Activity of a Selenourea Coordinated Gold(I)-Carbene Complex

Adam A. A. Seliman[a,b], Mohammad Altaf[c], Nurudeen A. Odewunmi[a], Abdel-Nasser Kawde[a], Wiktor Zierkiewicz[d], Saeed Ahmad[e], Saleh Altuwaijri[f], Anvarhusein A. Isab[a]*

[a]Department of Chemistry, King Fahd University of Petroleum and Minerals, Dhahran 31261, Saudi Arabia.
[b]Department of Chemistry, Al-Neelain University, Khartoum 11121, Sudan.
[c]Center of Excellence in Nanotechnology, King Fahd University of Petroleum and Minerals, Dhahran 31261, Saudi Arabia.
[d]Department of Chemistry, Wroclaw University of Technology, Wybrzeze Wyspianskiego 27, 50-370 Wroclaw, Poland.
[e]Department of Chemistry, College of Sciences and Humanities, Prince Sattam bin Abdulaziz University, Al-Kharj 11942, Saudi Arabia
[f]Clinical Research Laboratory, SAAD Research Development Center, SAAD Specialist Hospital, Al-Khobar 31952, Saudi Arabia

Abstract

A gold(I)-carbene complex, [Au(IPr)(Seu)]PF_6 (**1**), where Seu = Selenourea and IPr = 1,3-Bis(2,6-diisopropylphenyl)imidazol-2-ylidene, was prepared using [Au(IPr)Cl] and characterized by elemental analysis, IR, and NMR (^{1}H, ^{13}C, ^{77}Se) methods. The crystal structure of **1** was determined by single-crystal X-ray diffraction analysis, which shows that the complex (**1**) adopts a linear geometry about gold(I). The structures of the [Au(IPr)(Seu)]PF_6 monomer as a model of **1** and that of the dimer, {[Au(IPr)(Seu)]PF_6}$_2$ were optimized at the B3LYP-D3 level of theory. The DFT results give support to the experimentally determined monomeric structure. The *in vitro* cytotoxic activity of [Au(IPr)Cl] and complex **1** was investigated against three human cancer cell lines; A549(lung carcinoma), HCT15(colon cancer) and MCF7(breast cancer). The IC_{50} values showed that the selenourea-containing complex (**1**) was less potent than cisplatin in

inhibiting the growth of cancer cells. The stability of complex **1** in phosphate buffered aqueous solution and its interaction with amino acids; glutathione and L-cysteine were studied using square wave stripping voltammetry.

Keywords: Gold(I); carbene; selenourea; Crystal structure; Cytotoxicity

Corresponding author: aisab@kfupm.edu.sa

Introduction

Gold(I) complexes of *N*-heterocyclic carbenes (NHCs) have been studied extensively in recent years as prospective anticancer drug candidates. Several of them were found to exhibit remarkable cytotoxic properties, particularly in cisplatin-resistant cell lines [1-16]. The advantage of employing carbenes is that they make the resulting complexes more lipophilic and more stable with respect to ligand exchange reaction [17-19]. The lipophilicity of complexes can be tuned by varying the substituents on imidazole group. The presence of an ancillary ligand such as chloride, phosphine or thiol makes the complex more prone to ligand substitution reactions required for binding to the cellular targets [6,9,21-23]. With respect to the mechanism of antitumor action of gold(I) complexes, mitochondria involving selenoenzyme, thioredoxin reductase (TrxR) have been identified as the potential target sites [3,6-9,22,23]. The inhibition of the activity of thioredoxin reductase (TrxR) is associated with the induction of apoptosis in cancer cells. Several gold-NHC complexes as potent inhibitors of TrxR show strong antiproliferative effects on a broad spectrum of tumor cells [8,9,22-24].

The crystal structure studies on gold(I)-carbene complexes reveal a typical linear (quasi-) geometry for the central gold atom [4,12-16,25-32]. A number of gold(I) complexes based on diisopropylphenyl derivative of carbene (1,3-Bis(2,6-di-isopropylphenyl)imidazol-2-ylidene, Ipr) have been reported [2,15,25,29-32] and some of them were investigated for the anticancer properties [2,15]. The presence of isopropyl groups on carbene is expected to increase the lipophilicity of the resulting complex and thereby could enhance its cytotoxicity [2,6,22]. Therefore, we are interested in investigating the antitumor properties of gold(I) complexes of this particular carbene. In this regard, we have recently reported the crystal structures and anticancer properties of Ipr-Au-Dithiocarbamate complexes [15]. Here, we report the synthesis, spectral characterization and crystal structure of a new gold(I)-IPr complex having selenourea (Seu) as a co-ligand, [Au(Ipr)(Seu)]PF_6 (**1**). The cytotoxic activity of **1** against three human cancer cell lines; A549, HCT15, and MCF7, and its interaction with amino acids, L-tyrosine and L-tryptophan, were also investigated. So far, there is no known report in the literature on preparation of Au-carbene complexes having a selenium donor ligand. The structure of complex **1** and resonance assignment is shown in scheme 1.

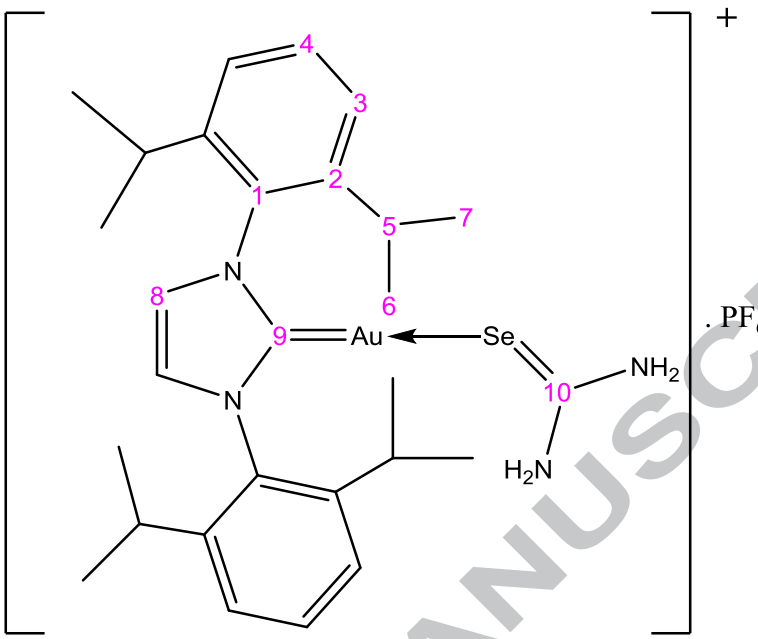

Scheme 1. Structure of [Au(IPr)(Seu)]PF_6 (**1**) and its resonance assignment

Experimental

Chemicals

The gold(I) precursor, chlorido[1,3-Bis(2,6-diisopropylphenyl)imidazol-2-ylidene]gold(I) {[Au(Ipr)(Cl)]}, selenourea, L-cysteine, enriched 99.9 % L-Cysteine (^{13}C), NaOD, DOCl glutathione and $AgPF_6$ were obtained from Sigma-Aldrich, St. Louis, USA.

Preparation of Complex 1

The complex **1** was prepared by mixing a solution of 0.127 g (0.500 mmol) $AgPF_6$ in 5 mL ethanol and 0.311 g (0.5 mmol) chlorido[1,3-Bis(2,6-diisopropylphenyl)imidazol-2-ylidene]gold(I), [Au(Ipr)(Cl)] in 5 mL CH_2Cl_2. After stirring for 5 minutes at room temperature the solution was filtered. To the filtrate, 0.0615 g (0.5 mmol) Seu was added. The solution was stirred for 1 hour and filtered. After three days, colorless crystals were obtained from the filtrate. Yield = 75%. Melting point = 195─198 ºC.

Analysis: Calcd. for $C_{28}H_{40}AuF_6N_4PSe$ (853.53 g/mol); C 39.60, H 4.72, N 5.56. Found; C 40.04, H 5.23, N 6.04.

Instrumentation

The solid state FTIR spectra were recorded on a Perkin-Elmer FTIR 180 spectrophotometer using KBr pellets over the range, 4000-400 cm^{-1}at resolution 4.0 cm^{-1}. The solution ^{1}H, ^{13}C and ^{77}Se NMR spectra in $CDCl_3$ were recorded on a LAMBDA LA-500 NMR spectrophotometer operating at the frequencies of 500.01, 125.65 and 200.0 MHz respectively. The spectral conditions for ^{13}C NMR were: 32 k data points, 0.967 s acquisition time, 1.00 s pulse delay and 45° pulse angle. The ^{77}Se NMR chemical shifts were recorded relative to an external reference ($NaHSeO_3$ in D_2O) at 1308.00 ppm using spectral condition: 2.00 s pulse delay and 0.311 s acquisition time.

The X-ray data of **1** was collected at 173K on a STOE IPSD II Image Plate Diffraction System connected with a two-circle goniometer and using MoKα graphite monochromator (λ= 0.71073 Å). The structure was solved by SHELXS-2014 program [33]. The refinement and further calculations were carried out with SHELXL-2014 [34]. The N-H H atoms were located in a Difference Fourier map and refined with a distance restraint of N-H = 0.88(2) Å and H…H = 1.40(2) Å. The C-bound H-atoms were included in calculated positions and treated as riding atoms: C-H = 0.95 - 1.0 Å with $U_{iso}(H)$ = $1.5U_{eq}(C)$ for methyl H atoms and = $1.2U_{eq}(C)$ for other H-atoms. The non-H atoms were refined anisotropically using weighted full-matrix least squares on F^2. A semi-empirical absorption correction was applied using the MULscanABS routine in PLATON [35]. The F atoms of the PF_6^- anion are disordered. The best solution was found by distributing the electron density over a total of 11 positions, which were refined with various fixed occupancy ratios to give a total of six F atoms. A summary of crystal data and structure refinement is given in reference [36].

Theoretical (DFT) calculations

Theoretical studies were performed for two model complexes, $[Au(IPr)(Seu)]PF_6$ (**1**) and its dimer, $\{[Au(IPr)(Seu)]PF_6\}_2$. In the case of both complexes, the fragments of the crystallographic structure were used as the initial geometries in the optimization procedures. The calculations were performed by using B3LYP-D3 method (standard hybrid density functional B3LYP [37,38] method with dispersion correction D3) [39] and combined basis sets LanL2DZ [40] for Au, Se and P atoms in conjunction with the D95V(d,p) [41] basis set for all other atoms. The atomic charges were calculated with

DFT method using the NBO program [42,43]. All computations were carried out with Gaussian 09 set of programs [44].

Measurement of Anticancer Activity

The complexes, [Au(IPr)Cl] and [Au(IPr)(Seu)]PF_6 (**1**) were tested for their, *in vitro* cytotoxic effects against human cell lines; MCF7 (breast cancer), HCT15 (colon cancer) and A549 (lung carcinoma) as reported previously [15]. The cells were seeded at the concentration of 3 x 10^3 cells/well in 100 µL of DMEM containing 10 % Fetal Bovine Serum (FBS) in a 96-well tissue culture plate and incubated for 72 h at 37 ^oC, 5% CO_2 and 90% relative humidity in a CO_2 incubator. After that 100 µL of 100, 50, 25 and 12.5 µM solutions of cisplatin and gold(I) complexes prepared in DMEM were added to the cells and the cultures were incubated for 72 h. The medium in the wells was cast off, and 100 µL of DMEM containing MTT (0.5 mg/ml) was added to the wells, with subsequent incubation in the CO_2 incubator at 37 ^{o} C in the dark for 4 h. After incubation, purple-colored formazan produced by the cells appeared as dark crystals in the bottom of the wells. The culture medium was carefully removed from each well to prevent disruption of the monolayer, and 100 µL of dimethylsulfoxide (DMSO) was added to each well. The solution in the wells was thoroughly mixed to dissolve the formazan crystals, which produce a purple solution. The absorbance of the 96 well-plates was measured at 570 nm with LabSystems Multiskan EX-ELISA reader against a reagent blank. The experimental results are calculated as the micromolar concentration of 50% cell growth inhibition (IC_{50}) of each drug. The MTT assay was carried out in three independent experiments for each analysis.

Electrochemical Measurements

Electrochemical (Square wave stripping voltammetry, SWSV) measurements were performed on a CH Instrument (CHI 1232A) potentiostat. Electrochemical cell comprises of; a platinum wire as a counter electrode, an Ag/AgCl saturated with KCl as reference electrode and glassy carbon electrode (GCE; 3.0 mm diameter, Model CHI104, CH Instruments, Austin, TX) as a working electrode inserted into 2.0 mL glass cell containing phosphate buffer solution, pH 7.0 as supporting electrolyte. 0.1 M buffer solution was prepared by mixing appropriate volumes of 0.2 M monosodium phosphate and disodium

phosphate prepared with double distilled water. Stock solutions of the complex prepared in methanol, while glutathione and L-cysteine were prepared with double distilled water. GCE was polished with 0.05 μm alumina, rinsed with distilled water prior to every SWSV measurements at room temperature in a quiescent condition at potential windows between -0.20 V and 1.20 V for the stability and interaction studies. Working conditions are; pulse width (increment) 4 mV, pulse height (amplitude) 25 mV and frequency, 15 Hz.

Results and Discussion

Spectroscopic Studies

The experimental IR spectrum of [Au(IPr)(Seu)]PF_6, in the range 4000 - 500 cm^{-1} is shown in Figure 1S. The vibrational frequencies and IR intensities were computed for the model [Au(IPr)(Seu)]PF_6 complex investigated. The B3LYP-D3 calculated vibrational frequencies and IR intensities as well as the bands observed in the experimental IR spectrum along with their assignments are collected in Table 1S. The vibrational assignment of the experimental spectrum was performed by examination of the calculated atomic displacements and visualization of the normal modes of the model [Au(IPr)(Seu)]PF_6 complex. As follows from the Table S1 and Figure S1, the band at 607 cm^{-1} is assigned to C═Se stretching vibration, which is shifted towards lower wave number with respect to its position in free Seu (736 cm^{-1}). This shift indicates a decrease in the double bond character of C═Se bond upon coordination. The calculated value of this mode in the complex is 635 cm^{-1}. The N─H stretching shows a shift to higher frequency region (3468, 3363 *Vs* 3453, 3265 cm^{-1} for free Seu). The N-H bending vibration of Seu in **1** was detected at 1635 cm^{-1}. Weak signals at 2960 & 3073 cm^{-1} for [Au(IPr)Cl] and 2960 & 3160 cm^{-1} for [Au(IPr)(Seu)]PF_6 due to C–H stretching vibrations of IPr were also observed.

The ^{1}H and ^{13}C NMR chemical shifts of the complexes are given in Tables 2S and 1 respectively. The values for [Au(Ipr)Cl] are close to those reported in the literature [15,30] and are presented here for comparison. The ^{1}H chemical shifts associated with IPr part of **1** fall in nearly the same region as observed for [Au(Ipr)Cl]. However, the N-H resonance of Seu in **1** shifted downfield by about 0.6 ppm compared to its value in the

free state. In ^{13}C NMR of [Au(IPr)(Seu)]PF_6 (**1**), the carbene carbon resonance shifted downfield by 10 ppm with respect to its position in [Au(IPr)Cl]. The downfield shift is consistent with the transfer of electron density from carbon to metal atom upon coordination. The other resonances of IPr ligand remained almost unchanged. On the other hand, the C=Se resonance in [Au(IPr)(Seu)]PF_6 appeared upfield by 9 ppm compared to that in uncoordinated Seu. This upfield shift is in accordance with the literature data [45-48].

In ^{77}Se NMR the coordination of Seu with gold(I) shifted the signal significantly upfield by more than 45 ppm ($\delta^{77}Se$ = 154.2 ppm in **1** *Vs* $\delta^{77}Se$ = 200.7 ppm in Seu). This very large shielding appears to be the characteristic of gold(I) binding to the selenium of Seu. This observation is consistent with the data of our previous studies [46-48].

Table 1 ^{13}C NMR chemical shifts (ppm) for Seu and gold(I) complexes in $CDCl_3$**.**

Compound	C1	C2	C3	C4	C5	C6	C7	C8	C=Au	C=Se
[Au(Ipr)Cl]	145.5	133.9	124.2	130.7	28.8	24.5	24.0	123.0	175.3	-
1	145.8	133.8	124.2	131.6	28.8	24.5	23.8	123.5	185.3	173.2
Seu	-	-	-	-	-	-	-	-	-	182.2

Description of X-ray Structure

The molecular structure and crystal packing of [Au(Ipr)(Seu)]PF_6 (**1**) are depicted in Figures 1 and 2 respectively. The selected bond lengths and angles for complex **1** are given in Table 2. The gold(I) atom in **1** is two-coordinate in a nearly linear environment with the C-Au-Se bond angle of 177.39(9)^o. The Au–C bond length (2.005(3) Å) falls in the range observed for other gold(I)-carbene complexes [25-32], while the Au–Se bond length (2.4089(6) Å) is somewhat shorter than that observed in the analogous phosphine complexes ((2.4360(6) Å [Me_3P-Au-Seu]$_2Cl_2$ [49] and 2.412(2) Å for [Ph_3P-Au-Seu]Cl [50]). The slightly shorter Au-Se bond suggests the stronger π-accepting ability of Seu in the presence of a carbene coordinated to gold. The complex **1** exists in the monomeric form similar to [Ph_3P-Au-Seu]Cl [50]. On the other hand, [Me_3P-Au-Seu]$_2Cl_2$ is a dinuclear complex assembled through aurophilic interactions (Au-Au = 3.0386(5) Å) [49]. In the case of **1** and [Ph_3P-Au-Seu]Cl, the dimerization is probably hindered by the steric effect of the bulky ligands. The C-Se bond length in **1** is slightly longer, while the

C-N distance is shorter than in the free Seu ligand (1.86(2) and 1.36 Å respectively) [51]. This observation is related to the N→C(Se) shift of electron density upon coordination and is consistent with the spectroscopic data. The SeCN2 moiety of Seu attains a trigonal planar environment. The complex cation and PF_6^- anion are associated with each other through electrostatic interactions.

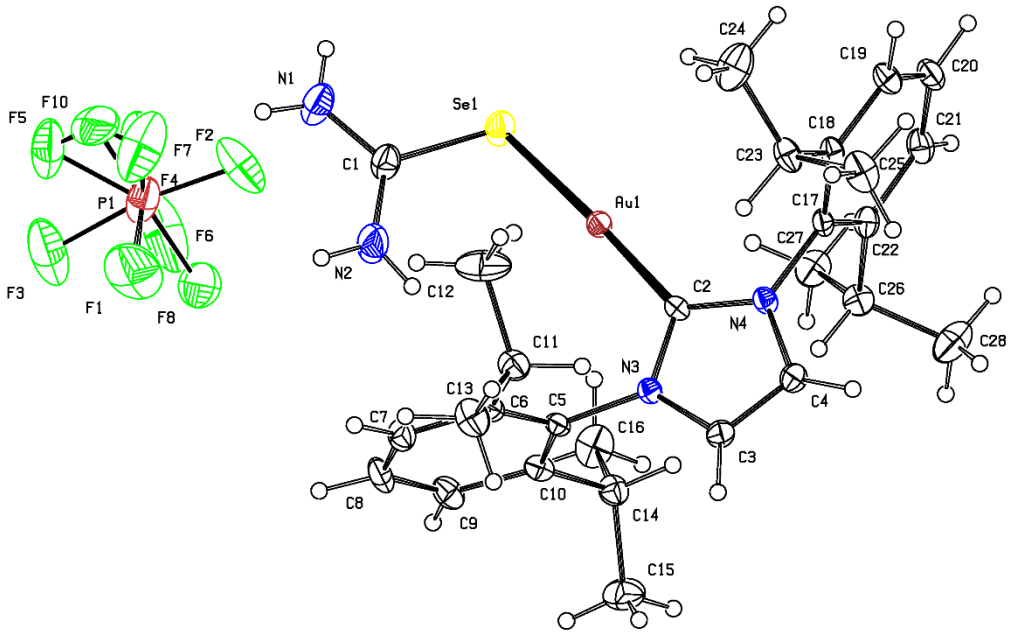

Figure 1 The molecular structure of [Au(Ipr)(Seu)]PF_6 (**1**) with atomic labeling. The displacement ellipsoids are drawn at the 30% probability level (F atoms of the PF_6^- anion are disordered). Selected structural parameters (interatomic distances in Å, bond angles in degrees) of [Au(IPr)(Seu)]PF_6 (**1**). Interatomic distances: Au1─C2 = 2.005(3); Au1─Se1= 2.4089(6); Se1─C1 = 2.883(4); N1─C1= 1.308(6); N2─C1= 1.320(7). Bond angles : Se1—Au1—C2= 177.39(9); Au1—Se1—C1= 99.67(14); N1—C1—N2= 119.80(4); Se1—C1— N1= 118.60(3); Se1—C1—N2= 121.50(3).

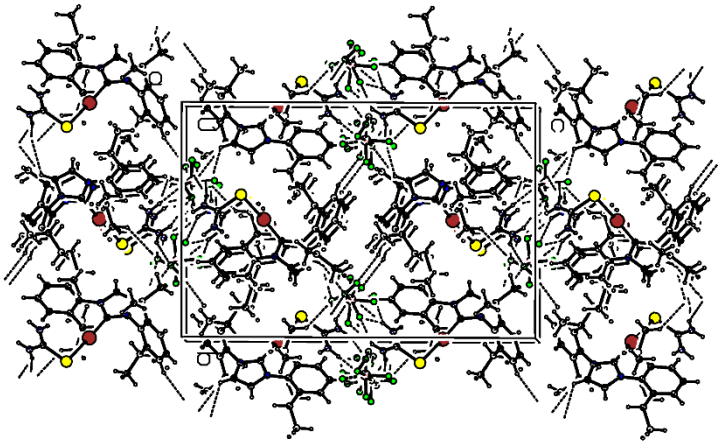

Figure 2 The crystal packing of [Au(Ipr)(Seu)]PF_6 (**1**) viewed along the *a* axis.

237 **Table 2** Selected structural parameters (interatomic distances in Å, bond angles in
238 degrees) of [Au(IPr)(Seu)]PF_6 (**1**).

Parameter	Exp.[a]	Theory
bond distances		
Au1-C2	2.005(3)	2.028
Au1-Se1	2.4089(6)	2.538
Se1-C1	2.883(4)	1.940
N1-C1	1.308(6)	1.334
N2-C1	1.320(7)	1.329
bond angles		
Se1—Au1—C2	177.39(9)	173.03
Au1—Se1—C1	99.67(14)	95.39
N1—C1—N2	119.80(4)	119.91
Se1—C1— N1	118.60(3)	118.17
Se1—C1—N2	121.50(3)	121.87

239 [a] Experimental values. [b] Theoretical values calculated at the DFT (B3LYP-D3) level of
240 theory.

DFT Calculations

Figure 2S shows the fully DFT optimized structure of $[Au(IPr)(Seu)]PF_6$ as the model complex of **1**. It has been found quite similar to that obtained in the experiment (see Figure 1).

The selected, experimentally determined and B3LYP-D3 calculated interatomic distances and bond angles of the $[Au(IPr)(Seu)]PF_6$ (**1**) complex are listed in Table 2. According to the results presented in Table 2, all but one of the calculated interatomic distances are slightly overestimated with respect to that determined experimentally. The only exception is the Se1-C1 interatomic distance, where the calculated value is shorter by 0.0.943 Å than the X-ray determined value. As follows from the results presented in Table 2, the calculated values of the bond angles are similar to these found in the X-ray structure.

The complex **1** exists in the monomeric form. On the other hand, the analogous phosphine complex, $[Me_3P\text{-}Au\text{-}Seu]_2Cl_2$ is a dinuclear complex assembled through aurophilic interactions (Au-Au = 3.0386(5) Å) [49]. In this work, the question arises, whether the **1** complex is able to form a dimer stabilized by the Au-Au interaction. To answer this question we tried to form a dimer similar to the $[Me_3P\text{-}Au\text{-}Seu]_2Cl_2$ dimer. In Figure S3, the two structures of the $\{[Au(IPr)(Seu)]PF_6\}_2$ dimers are shown. One of them is optimized. In this case the fragment of the crystallographic structure was used as the initial geometries in the calculations. In this complex the Au-Au distance is 6.817 Å. The second structure was constrained as in $[(Me_3P\text{-}Au\text{-}Seu)_2^{2+}\ 2Cl^-]$ dimer. Unfortunately, the dimer of **1** stabilized by the Au-Au interaction (where the Au-Au distance is 3.039 Å) is impossible due to ligand overlap (see Figure 3S).

NBO charges

The NBO charges on selected atoms of the studied complex as well as of the isolated ligand are reported in Table 3S. As follows from this table the charge on the Au1 ion is 0.21 e. This value is similar to that calculated on the gold(I) ion in the Au(I) complex with 1,3-dioxane and $P(OMe)_3$ [18]. In this complex, the NBO charge on the metal center calculated with M06 functional is equal to 0.23 e [18]. In the complex (**1**), the natural electron configuration of the Au(I) is: [core] $6S^{0.92}\ 5d^{9.72}\ 6p^{0.13}$. Thus, 68 core electrons, 10.77 valence electrons (on 6s, 5d and 6p orbitals) and 0.02 e on the Rydberg orbitals

($6d^{0.01}$ $7p^{0.01}$) give the total of 78.79 electrons on the Au cation. This is consistent with the calculated NBO charge on this cation (the difference between the nuclear charge (Z) 79 and 78.79 e).

According to the DFT calculations, the charges on the Se1 and C2 atoms bound to the central cation are -015 and 0.17 e, respectively (see Figure S2). These charges are more positive than those calculated in the isolated ligands by 0.05 and 0.01 e, respectively. With respect to the carbon atom (C1) of Seu ligand, the charge on it is 0.37 e. Upon complexation, the charge on this atom increases by 0.12 e. As follows from the Table S3, the charges on the N1 and N2 atoms also increase upon complexation. An increase on each of these nitrogen atom amounts to 0.05 e.

According to the NBO results, in the [Au(IPr)(Seu)]PF_6 model complex (**1**) there are weak interactions between gold(I) and four H atoms of the methyl groups. The strength of each of these interactions estimated by the second-order interaction energy E^2 is about 0.17 kcal mol^{-1}.

Evaluation of Anticancer Activity

The complexes, [Au(Ipr)Cl] and [Au(Ipr)(Seu)]PF_6 (**1**), as well as cisplatin (standard anticancer drug), were tested for *in vitro* cytotoxicity against three human cancer cell lines; A549 (lung carcinoma), HCT15 (colon cancer cells) and MCF7 (breast cancer cells) using MTT assay. The IC_{50} values (as μM) obtained from the plot of the concentration of compounds against the percentage of cell viability are given in Table 3. The dose-dependent inhibition of cell proliferation was obtained by a specific increase in the concentration of cisplatin and gold complexes against a fixed number of three human cancer cell lines as illustrated in Figure 3. The data in Table 3 showed that the gold complexes with higher IC_{50} values were less effective than cisplatin in inhibiting the growth of cancer cells in all cases. However, complex **1** is more active than [Au(IPr)Cl]. The greater activity of **1** compared to [Au(IPr)Cl] suggests that the binding of Seu increases the inhibition efficiency of the gold(I) complex. This may be due to the ionic nature of the complex that favors its aqueous solubility. The effectiveness of the complexes is almost same for the three cells. Recently, we reported the cytotoxic properties of gold(I) complexes of 2-aminoethyldiphenylphosphine (AEP), [Au(AEP)Cl] and [$Au(AEP)_2$]Cl against the same cell lines [52]. A comparison of the activities reflects that complex **1** is less effective. Among the AEP complexes, the ionic complex is more

active, which indicates that the ionic nature along with the lipophilic properties of the ligands make the complex better a anticancer agent. The lower activity of **1** may be due to the steric bulk of the IPr ligand. Therefore, it is assumed that the activity of the complexes is related to the structure and composition of the complexes.

Table 3 IC_{50} values (μM) of gold(I) complexes against HCT15, A549 and MCF7 cancer cell lines

Complex	HCT15	A549	MCF7
Cisplatin	32 ± 2	42 ± 2	23 ± 4
[Au(Ipr)Cl]	122 ± 1	180 ± 2	110 ± 2
1	76 ± 2	82 ± 1	75 ± 3
[Au(AEP)Cl][a]	51.21 ± 0.83	53.97 ± 0.94	38.34 ± 0.22
$[Au(AEP)_2]Cl$[a]	34.19 ± 2.49	34.42 ± 1.02	51.73 ± 2.25

[a] Data from ref. 52

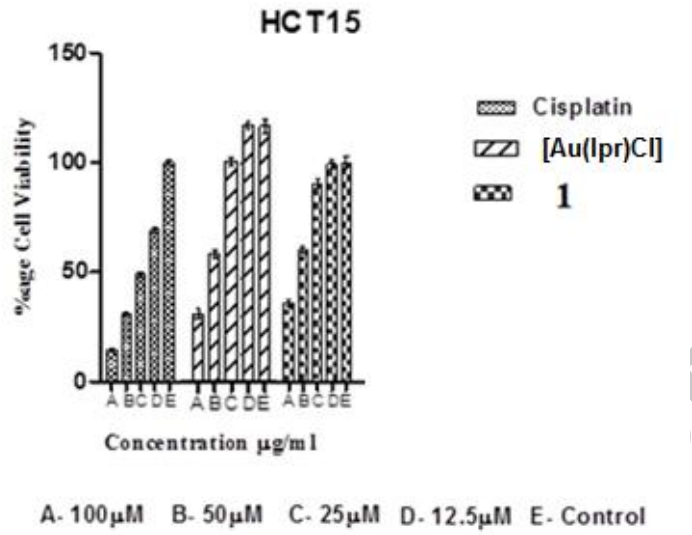

315

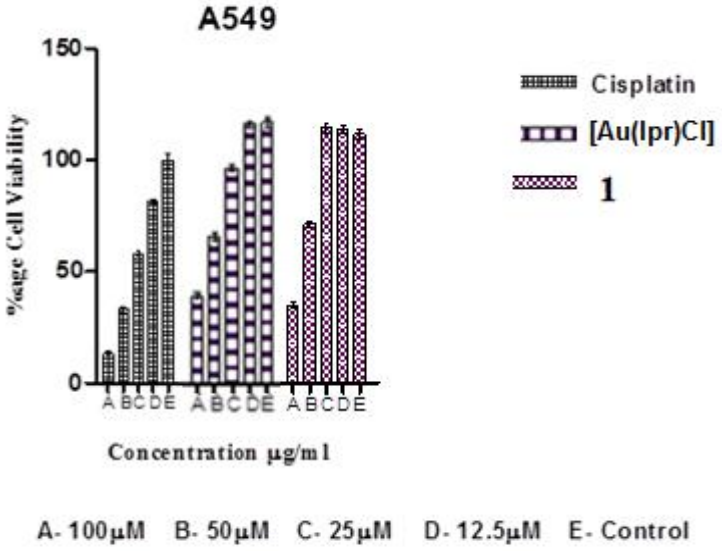

316

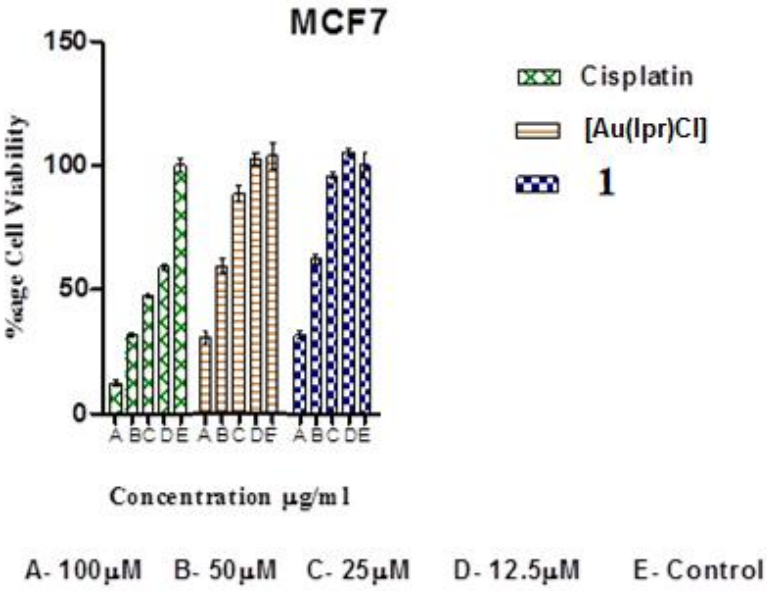

317

318 **Figure 3** The survival of the cells as a function of concentration of the complexes

Electrochemical Studies

Stability and Electrochemical behavior

The stability and electrochemical behavior of complex **1** were examined by its electroactive properties in phosphate buffer solution of pH 7.0 using SWSV technique (Square wave stripping voltammetry). In order to obtain the best electrochemical response, a preliminary study was carried out using relevant reference solutions (phosphate buffer aqueous solution and methanol). Two oxidized peaks on the surface of a glassy carbon electrode (GCE) at about 0.20 V and 0.60 V were observed for complex **1** as shown in Figure 4. These peaks may likely be the result of free electron transfer from the solution of the complex to the surface of the electrode by applying potential. Intensities of both peaks were observed to raise with the presence of successive addition of 100 μL of 25, 50, 75 and 100 μMs concentrations of complex **1** in 0.1 M phosphate buffer (pH 7.0) complex solution in 2.0 mL total solution. The complete solubility of the studied concentrations of the complex in the medium is responsible for the increase in peak height with an estimation of 8.53 mg/100 ml solubility of complex **1** in phosphate buffer based on the highest soluble concentration. A stock solution of 0.5mM of the complex in methanol stored for about 8 weeks at room temperature without coagulation of the complex and the perseverance of peaks at different concentration levels in phosphate buffer solution is an evidence of the stability of the complex.

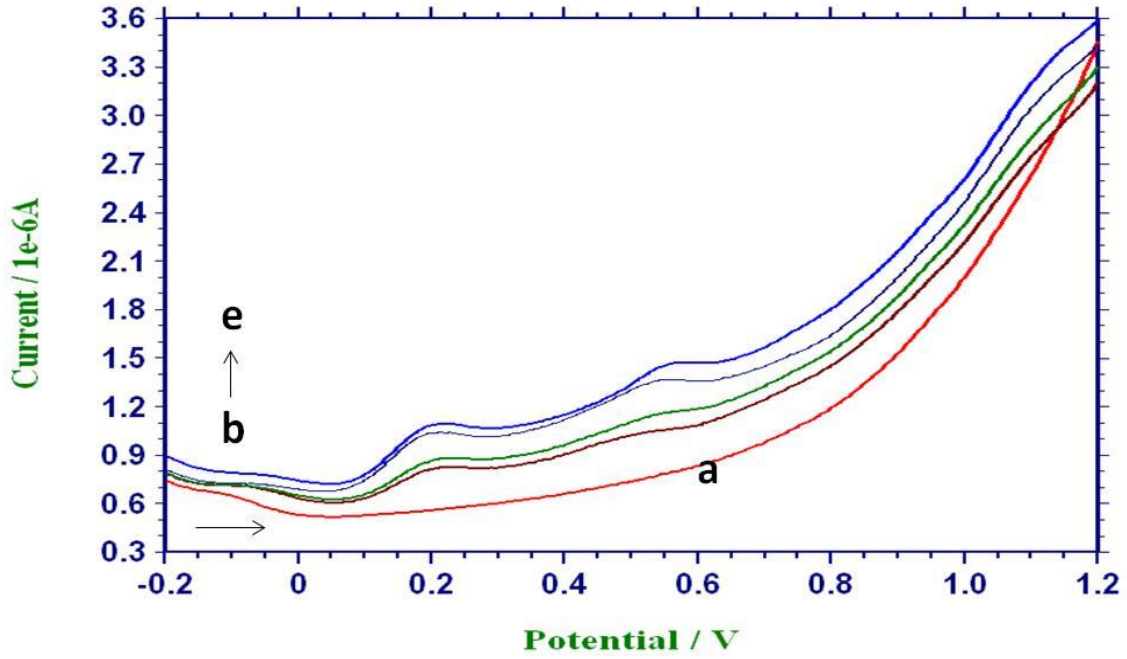

Figure 4 SWS voltammograms of 0.1 M phosphate buffer aqueous solution (2.0 mL) at GCE (a) and in the presence of 0.10 mL, 25.0 µM (b), 0.20 mL, 50.0 µM (c), 0.30 mL, 75.0 µM (d) and 0.40 mL, 100.0 µM (e) of the complex**.**

Interaction Study of Complex 1 with Glutathione and L-Cysteine

However, drug-protein interaction seems ambiguous due to structural complexability of protein. Interaction studies of the drug are essential to investigate the binding of the drug with protein and its transportation to the target site. Consequently, physicochemical properties of amino acids and small sizes peptide bond molecule have been used to understand drug-protein interaction [53], which makes glutathione and L-cysteine a good choice as model compounds for drug-protein interaction due to their role in cancer diagnosis and therapy [54,55].

Voltammograms obtained for the interaction studies of the complex (**1**) with glutathione and L-cysteine are shown in Figure 5 and 6 respectively. Figure 5A shows the effect of the addition of methanol in the absence of complex **1** on 0.2 mM glutathione as a control experiment for Figure 5A[l]. Continuous reduction in the peak of glutathione (Figure 5Ab) can be observed in Figure 5Ac – 5Af as a result of the subsequent addition of 100 µL methanol to the solution. These reductions in the peak can be attributed to dilution of the glutathione concentration. However, when the same volumes of methanol

in the presence of 25, 50, 75 and 100 μMs concentrations (Figure 5A^{l}d - 5A^{l}g) of the complex were added, shift towards a positive potential and increase in current peaks of both peaks attributed to complex **1** (Figure 4) were observed when compared with the position and current peak 100 μM concentration of the complex (Figure 5A^{l}c). These behaviors clearly show that interaction between glutathione and complex **1** is responsible for the shift in peak position and change peak height of the complex and that methanol does not contribute to the interaction. To further justify the interaction, another control experiment involving the serial addition of 40 μL double distilled into 100 μM complex **1** is shown in Figure 5B for 5B^{l} to investigate the effect of glutathione concentration on complex 1. Reduction in the peaks of 100 μM complex **1** (Figure 5Bb) can be observed in Figure 5Bc – 5Be as a result of the dilution in complex **1** concentration. Besides, when the same volume containing 0.2, 0.4 and 0.6 mM concentrations (5B^{l}d - 5A^{l}f) were added subsequently to 100 μM complex **1**, huge increase in the current peaks compared to Figure 5B^{l}c (100 μM complex **1**) was observed to confirm the interaction of glutathione and complex **1**.

Another form of interaction of complex **1** was observed when similar studies were performed with L-cysteine (Figure 6). Obvious dilutions of 0.2 mM L-cysteine were observed with methanol control experiment (Figure 6A). Drastic reductions in the peak of L-cysteine (Figure 6Ab) can be observed in Figure 6Ac – 6Af as a result of the subsequent addition of 100 μL methanol to the solution. In contrast to the interaction pattern of glutathione observed in figure 5A^{l}, there is a reduction in the peak of L-cysteine with the appearance of two new peaks of a wider potential shift when compared with Figure 6A^{l}c of 100 μM complex **1**. Interestingly, the peak at about 0.15 V was showing a reduction in peak current, and the other peak at about 0.70V was showing an increase in a number of peaks as the concentration of complex **1** from 25 - 100 μM as shown in Figure 6A^{l}d - 6A^{l}g. This complexity of complex **1** peak in the presence of L-cysteine is also a proof of it interaction with complex **1**. The interaction was further investigated with different concentration of L-cysteine with a control experiment with double distilled water (Figure 6B, same as 5B). Equal volume of distilled water used in the control experiment but containing 0.2, 0.4 and 0.6 mM concentrations of L-cysteine (6B^{l}d - 6A^{l}f) were added subsequently to 100 μM complex **1**, an increase in the current peaks compared to Figure 6B^{l}c (100 μM complex **1**) were observed to confirm the interaction of L-cysteine and complex **1**.

Multiple isoenzymes (IE) which are a significant evidence of polymorphic variation functionality is the main constituent of glutathione S-transferases (GSTs). Expression pattern of IE is a determining factor in cancer treatment and susceptibility [54,55). Interaction of complex **1** with glutathione is an evidence of its ability to bind with protein and thereby aid the regulation of mitogen- activated protein kinases (MAPK) for the transportation of drug to the target site. The interaction can initiate S-glutathionylation which is the addition of glutathione to the residue cysteine in the target protein. Apart from the binding of the complex with protein, the possibility of its efficiency is demonstrated by its interaction with L-cysteine.

403

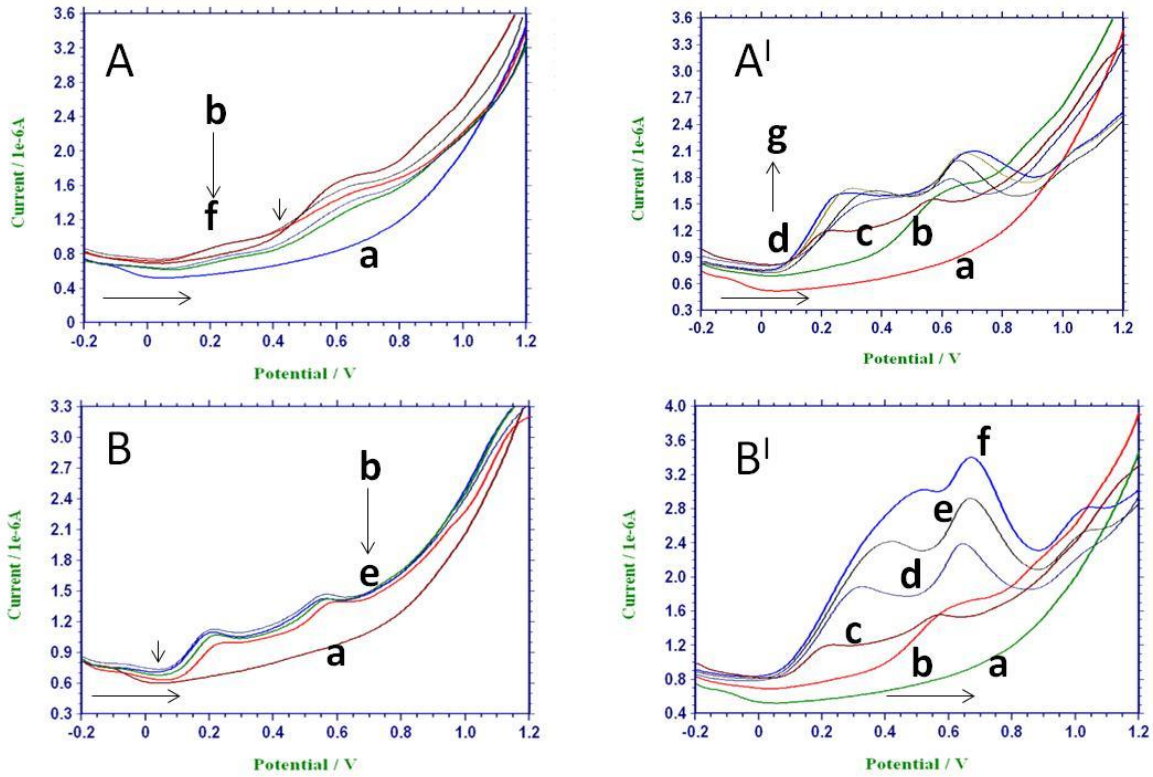

404

405 **Figure 5.** SWS voltammograms of 0.1 M phosphate buffer (pH 7.0) aqueous solution (2.0
406 mL) at a GCE surface;(A) effect of solvent (methanol) on glutathione as a control
407 experiment for A ^{I}, (A ^{I}) effect of complex on glutathione; blank solution (a), 0.04 mL,
408 0.2 mM glutathione(b), 0.40 mL, 100 µM complex without glutathione (c) , 0.10 mL,
409 25.0 µM (d), 0.20 mL, 50.0 µM (e), 0.30 mL, 75.0 µM (f) and 0.40 mL, 100.0 µM (g) of
410 the complex in the presence of 0.04 mL, 0.2 mM glutathione. (B) effect of solvent
411 (water) on complex as a control experiment for B ^{I}, (B ^{I}) effect of different
412 concentrations of glutathione on 0.40 mL, 100 µM complex ; blank solution(a) 0.04 mL,
413 0.2 mM glutathione (b), 0.40 mL, 100 µM complex without glutathione (c) , 0.04 mL,
414 0.2 mM (d), 0.08 mL, 0.4 mM (e) and 0.12 mL, 0.6 mM (f) of glutathione in the presence
415 of 0.40 mL,100 µM complex.

416

417

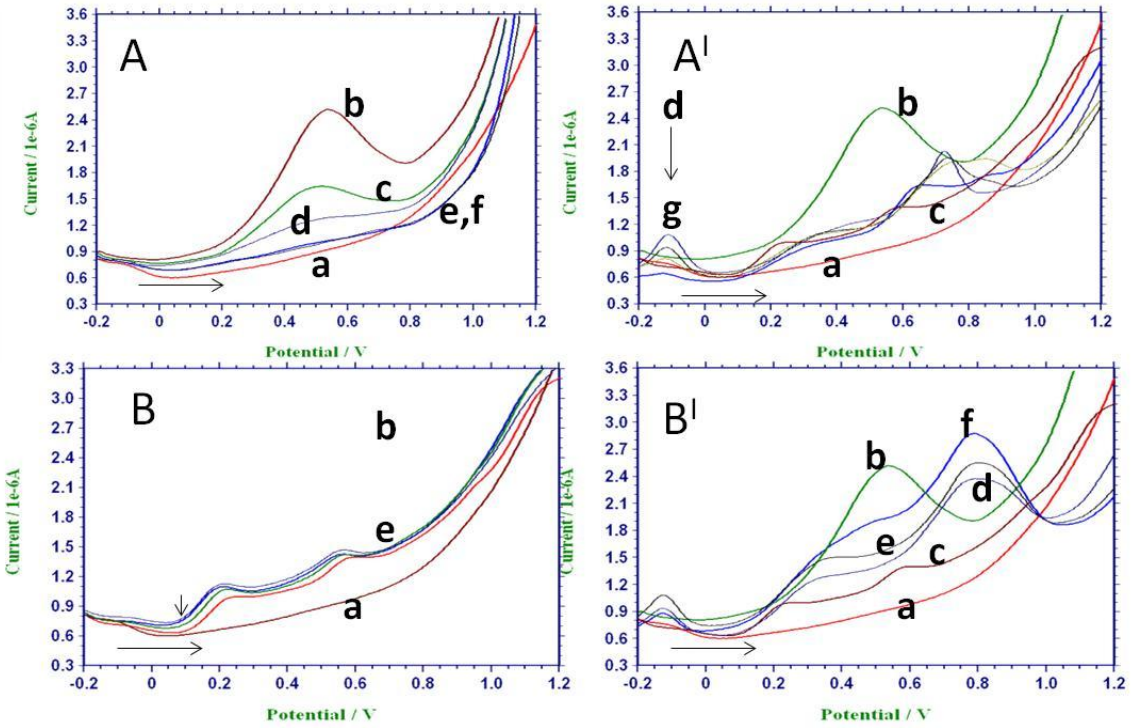

418

419 **Figure 6**. SWS voltammograms of 0.1 M phosphate buffer (pH 7.0) aqueous solution (2.0
420 mL) at a GCE surface;**(A)** effect of solvent (methanol) on L-cysteine as a control
421 experiment for **A ^{I} , (A ^{I})** effect of complex on L-cysteine; blank solution **(a)**, 0.04 mL,
422 0.2 mM L-cysteine **(b),** 0.40 mL, 100 µM complex without L-cysteine **(c) ,** 0.10 mL,
423 25.0 µM **(d),** 0.20 mL, 50.0 µM **(e),** 0.30 mL, 75.0 µM **(f)** and 0.40 mL, 100.0 µM (g) of
424 the complex in the presence of 0.04 mL, 0.2 mM L-cysteine. **(B)** effect of solvent (water)
425 on complex as a control experiment for B ^{I} **, (B ^{I})** effect of different concentrations of
426 glutathione on 0.40 mL, 100 µM complex ; blank solution**(a)** 0.04 mL, 0.2 mM L-
427 cysteine **(b),** 0.40 mL, 100 µM complex without L-cysteine **(c) ,** 0.04 mL, 0.2 mM (d),
428 0.08 mL, 0.4 mM (e) and 0.12 mL, 0.6 mM (f) of L-cysteine in the presence of 0.40 mL,
429 100 µM complex.

430

Interaction Study of Complex 1 with enriched L-Cysteine using ^{13}C NMR Spectroscopy

Interaction of complex **1** with 99.9 % ^{13}C-enriched L-Cysteine was carried out in D_2O at pH 7.5 using different concentrations of L-Cysteine. The reaction products were monitored by ^{13}C and NMR as shown in Figure 7. Fig. 7A shows the ^{13}C NMR spectrum of 8.5 mg (1.0 eq.) of complex **1,** and Fig. 7B that of L-Cysteine (^{13}C-enriched) with chemical shifts at 167.58, 41.59, 27.47 ppm for a, b and c respectively. When enriched L-Cysteine (1.21 mg, 1.0 eq.) was added to (1.0 eq.) of complex **1**, the color of the solution changed to faint yellow and the ^{13}C NMR peaks of enriched L-Cysteine were observed downfield at 171.28, 43.30, 34.98 ppm for a, b and c respectively (Fig. 7C) due to complexation. Whereas, the peak observed at 180.81 ppm represent the free Seu ligand and the species [Au(Ipr)(L-Cys)]. Upon addition of L-Cysteine to complex **1** at complex: L-CysH (1:2) equivalent, a yellow solution was observed that later changed to red color after 72 hours due to the reduction of Seu to metallic Selenium as shown in Fig.7D. All ^{13}C NMR peaks of IPr moiety shifted downfield. The signal due to L-Cysteine moiety remained constant, the C=Au resonance was observed more shielded. Three new peaks at 175.78 ppm, 187.32 ppm, and 188.39 ppm, which appeared in the spectrum may be due to different coordination geometry around Au(I) ion [56]. The ^{13}C NMR chemical shifts of different species in the interaction progress are shown in Table 4.

Table 4 ^{13}C NMR chemical shifts (ppm) for the reaction complex **1** with Seu in D_2O.

Molar ratio	Specie	C=Au	C=Se	-C(O)(OH)	>C-S-	>C*-NH_2
-	[Au(Ipr)Cl]	175.3	-	-	-	-
Complex **1** (1:0)	$[Au(Ipr)(Seu)]^+$	185.3	173.2	-	-	-
(1:1)	[Au(Ipr)(L-Cys)]	185.2, 184.8	180.8	171.2	34.9	43.3
(1:2)	[Au(Ipr)(L-Cys)]	188.3, 187.3	-	172.5, 175.7	32.4 31.6	43.0
L-Cysteine	-	-	-	167.5	27.4	41.5
Free Seu	-	-	182.2	-	-	-

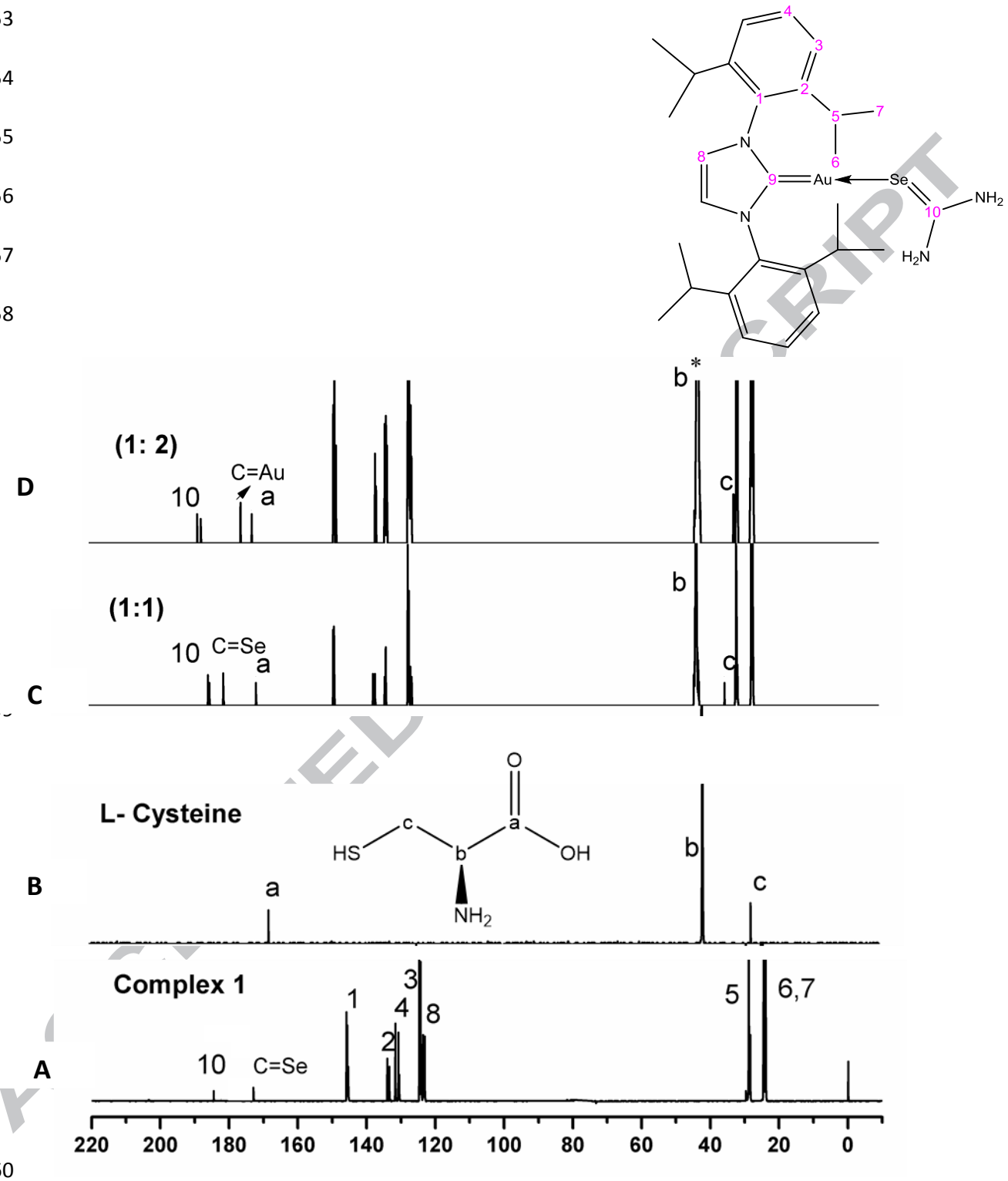

Figure 7. ^{13}C NMR spectra for: free complex 1 (**A**), free enriched L-Cysteine (**B**), reaction of complex **1** with enriched L-Cysteine at 1:1(**C**), and at 1:2 (**D**). All spectra were recorded in D_2O at pH 7.5 and at ambient room temperature.

Conclusion

In this study, we have reported the first crystal structure of an adduct formed between gold(I)-carbene compound and selenourea, [Au(IPr)(Seu)]PF_6 (**1**). The spectral characterization and *in vitro* cytotoxicity of complex **1** was described. Single crystal X-ray diffraction revealed that complex **1** exhibited a distorted linear geometry at gold. The DFT calculations support that the experimentally determined structure (**1**) is more stable in comparison to the dimeric structure, {[Au(IPr)(Seu)]PF_6}$_2$. The complex (**1**) was found to be less potent as an anticancer agent than cisplatin against A549, HCT15, and MCF7 human cancer cell lines. It is stable in aqueous solution within 72 h and shows a clear interaction with glutathione and L-cysteine due to Au (I) soft lewis acid property for effective S-glutathionylation.

Acknowledgement

The authors greatly appreciate and thank the financial support provided by King Fahd University of Petroleum and Minerals under the project No. **IN151022**.

This work was also financed in part by a statutory activity subsidy from the Polish Ministry of Science and Higher Education for the Faculty of Chemistry of Wroclaw University of Technology. A generous computer time from the Wroclaw Supercomputer and Networking Center is acknowledged.

Supplementary information

CCDC 1522006 for the complex **1** contains the supplementary crystallographic data for this paper. These data can be obtained free of charge from The Cambridge Crystallographic Data Centre via www.ccdc.cam.ac.uk/data_request/cif

References

1. B. Bertrand, A. Casini, A golden future in medicinal inorganic chemistry: the promise of anticancer gold organometallic compounds, Dalton Trans. 43 (2014) 4209–4219.

2. J. Weaver, S. Gaillard, C. Toye, S. Macpherson, S. P. Nolan, A. Riches**,** Cytotoxicity of Gold(I) N-Heterocyclic Carbene Complexes Assessed by Using Human Tumor Cell Lines, Chem.- Eur. J. 17 (2011) 6620 – 6624.

3. Y. Li, G.-F. Liu, C.-P. Tan, L.-N. Ji, Z.-W. Mao, Antitumor Properties and Mechanisms of Mitochondria-Targeted Ag(I) and Au(I) Complexes Containing N-Heterocyclic Carbenes Derived From Cyclophanes, Metallomics 6 (2014) 1460-1468.

4. H. Sivaram, J. Tan, H.V. Huynh, Syntheses, Characterizations, and a Preliminary Comparative Cytotoxicity Study of Gold(I) and Gold(III) Complexes Bearing Benzimidazole- and Pyrazole-Derived N-Heterocyclic Carbenes, Organometallics 31 (2012) 5875-5883.

5. A. Pratesi, D. Cirri, M. D. Duovic, S. Pillozzi, G. Petroni, Z. D. Bugarcic, L. Messori, New gold carbene complexes as candidate anticancer agents, Biometals 29 (2016) 905-911.

6. P. J. Barnard, M. V. Baker, S. J. Berners-Price, A. D. Day, Mitochondrial permeability transition induced by dinuclear gold(I)–carbene complexes: potential new antimitochondrial antitumor agents, J. Inorg. Biochem. 98 (2004) 1642–1647.

7. L. Messori, L. Marchetti, L. Massai, F. Scaletti, A. Guerri, I. Landini, S. Nobili, G. Perrone, E. Mini, P. Leoni, M. Pasquali, C. Gabbiani, Chemistry and Biology of Two Novel Gold(I) Carbene Complexes as Prospective Anticancer Agents, Inorg. Chem. 53 (2014) 2396–2403.

8. E. Schuh, C. Pfluger, A. Citta, A. Folda, M. P. Rigobello, A. Bindoli, A. Casini, F. Mohr, Gold(I) Carbene Complexes Causing Thioredoxin 1 and Thioredoxin 2 Oxidation as Potential Anticancer Agents, J. Med. Chem. 55 (2012) 5518–5528.

9. R. Rubbiani, E. Schuh, A. Meyer, J. Lemke, J. Wimberg, N. Metzler-Nolte, F. Meyer, F. Mohr, I. Ott, TrxR inhibition and antiproliferative activities of structurally diverse gold N-heterocyclic carbene complexes, Med. Chem. Commun. 4 (2013) 942-948.

10. J. Lemke, A. Pinto, P. Niehoff, V. Vasylyeva, N. Metzler-Nolte, Synthesis, structural characterization and anti-proliferative activity of NHC gold amino acid and peptide conjugates, Dalton Trans. (2009) 7063–7070.

11. B. Bertrand, A. Citta, I. L. Franken, M. Picquet, A. Folda, V. Scalcon, M. P. Rigobello, P. Le Gendre, A. Casini, E. Bodio, Gold(I) NHC-based homo- and heterobimetallic complexes, J. Biol. Inorg. Chem. 20 (2015) 1005–1020.

12. T. J. Siciliano, M. C. Deblock, K. M. Hindi, S. Durmus, M. J. Panzner, C. A. Tessier, W. J. Youngs, Synthesis and anticancer properties of gold(I) and silver(I) N-heterocyclic carbene complexes, J. Organomet. Chem. 696 (2011) 1066–1071.

13. B. Bertrand, L. Stefan, M. Pirrotta, D. Monchaud, E. Bodio, P. Richard, P. Le Gendre, E. Warmerdam, M. H. de Jager, G. M. M. Groothuis, M. Picquet, A. Casini, Caffeine-Based Gold(I)-*N*-Heterocyclic Carbenes as Possible Anticancer Agents: Synthesis and Biological Properties, Inorg. Chem. 53 (2014) 2296–2303.

14. B. K. Rana, A. Nandy, V. Bertolasi, C. W. Bielawski, K. D. Saha, J. Dinda, Novel Gold(I)– and Gold(III)–N-Heterocyclic Carbene Complexes: Synthesis and Evaluation of Their Anticancer Properties, Organometallics 33 (2014) 2544–2548.

15. M. Altaf, M. Monim-ul-Mehboob, A. A.A. Seliman, A. A. Isab, V. Dhuna, G. Bhatia, K. Dhuna, Synthesis, X–ray Structures, Spectroscopic Analysis and Anticancer Activity of Novel Gold(I) Carbene Complexes, J. Organomet. Chem. 765 (2014) 68-79.

16. B. Bertrand, E. Bodio, P. Richard, M. Picquet, P. Le Gendre, A. Casini, Gold(I) N-heterocyclic carbene complexes with an "activable" ester moiety: Possible biological applications, J. Organomet. Chem. 775 (2015) 124-129.

17. D. Marchione, L. Belpassi, G. Bistoni, A. Macchioni, F. Tarantelli, D. Zuccaccia, The Chemical Bond in Gold(I) Complexes with N-Heterocyclic Carbenes. Organometallics 33 (2014) 4200-4208.

18. D. Benitez, N. D. Shapiro, E. Tkatchouk, Y. Wang, W. A. Goddard, F. D. Toste, A bonding model for gold(I) carbene complexes, Nature Chem. 1 (2009) 482–486.

19. L. N. D. S. Comprido, J. E. M. N. Klein, G. Knizia, J. Kastner, A. S. K. Hashmi, The Stabilizing Effects in Gold Carbene Complexes, Angew. Chem. Int. Ed. 54, (2015) 10336 –10340.

20. M. V. Baker, P. J. Barnard, S. J. Berners-Price, S. K. Brayshaw, J. L. Hickey, B. W. Skelton, A. H. White, Synthesis and structural characterization of linear Au(I) N-heterocyclic carbene complexes: New analogues of the Au(I) phosphine drug Auranofin, J. Organomet. Chem. 690 (2005) 5625–5635.

21. R. Rubbiani, S. Can, I. Kitanovic, H. Alborzinia, M. Stefanopoulou, M. Kokoschka, S. Mönchgesang, W. S. Sheldrick, S. Wölfl, I. Ott, Comparative in Vitro Evaluation of N-Heterocyclic Carbene Gold(I) Complexes of the Benzimidazolylidene Type, J. Med. Chem. 54 (2011) 8646–8657.

22. M. V. Baker, P. J. Barnard, S. J. Berners-Price, S. K. Brayshaw, J. L. Hickley, B. W. Skelton, A. H. White, Cationic, linear Au(I) *N*-heterocyclic carbene complexes: synthesis, structure and anti-mitochondrial activity, Dalton Trans. (2006) 3708–3715.

23. J. L. Hickey, R. A. Ruhayel, P. J. Barnard, M. V. Baker, S. J. Berners-Price, A. Filipovska, Mitochondria-Targeted Chemotherapeutics: The Rational Design of Gold(I) *N*-Heterocyclic Carbene Complexes That Are Selectively Toxic to Cancer Cells and Target Protein Selenols in Preference to Thiols, J. Am. Chem. Soc. 130 (2008) 12570-12571.

24. X. Cheng, P. Holenya, S. Can, H. Alborzinia, R. Rubbiani, I. Ott, S. Wolfl, A TrxR inhibiting gold(I) NHC complex induces apoptosis through ASK1-p38-MAPK signaling in pancreatic cancer cells, Mol. Cancer 13 (2014) 221.

25. P. J. Barnard, M. V. Baker, S. J. Berners-Price, B. W. Skelton, A. H. White, Dinuclear gold(I) complexes of bridging bidentate carbene ligands: synthesis, structure and spectroscopic characterization, Dalton Trans. (2004) 1038 – 1047.

26. H. G. Raubenheimer, L. Lindeque and S. Cronje, Synthesis and characterization of neutral and cationic diamino carbene complexes of gold(I), J. Organomet. Chem. 511 (1996) 177–184.

27. M. Z. Ghdhayeb, R. A. Haque, S. Budagumpi, Synthesis, characterization and crystal structures of silver(I)– and gold(I)–*N*-heterocyclic carbene complexes having benzimidazol-2-ylidene ligands, J. Organomet. Chem. 757 (2014) 42-50.

28. E. Deck, K. Reiter, W. Klopper, F. Breher, A Dinuclear Gold(I) Bis(Carbene) Complex Based on a Ditopic Cyclic (Aryl)(Amino)Carbene Framework, Z. Anorg. Allg. Chem. 642 (2016) 1320–1328.

29. P. de Fremont, N. M. Scott, E. D. Stevens, S. P. Nolan, Synthesis and structural characterization of N-heterocyclic carbene gold(I) complexes, Organometallics 24 (2005) 2411-2418.

30. M. R. Fructos, T. R. Belderrain, P. de Fremont, N. M. Scott, S. P. Nolan, M. M. Diaz-Requejo, P. J. Perez, A Gold Catalyst for Carbene-Transfer Reactions from Ethyl Diazoacetate, Angew. Chem. Int. Ed. 44 (2005) 5284 –5288.

31. S. Gaillard, A. M. Z. Slawin, S. P. Nolan, A N-heterocyclic carbene gold hydroxide complex: a golden synthon, Chem. Commun. 46 (2010) 2742–2744.

32. A. Gomez-Suarez, R. S. Ramon, A. M. Z. Slawin, S. P. Nolan, Synthetic Routes to [Au(NHC)(OH)] (NHC = *N*-heterocyclic carbene) complexes, Dalton Trans. 41 (2012) 5461–5463.

33. G. M. Sheldrick, A short of SHELX, Acta Cryst. A64 (2008) 112-122.

34. G. M. Sheldrick, Crystal Refinement with SHELXL, Acta Cryst. C71 (2015) 3–8.

35. A. L. Spek, Structure validation in chemical crystallography, Acta Cryst. D65 (2009) 148-155.

36. Crystal data: $C_{28}H_{40}AuF_6N_4PSe$, Mw 853.53, Monoclinic, P 21/n; a 10.1086 (5), b 15.4507 (5), c 23.3372 (12) Å, β/96.407(4)°; V/3263.8(3) $Å^3$, D_{calc}/1.737 gm^{-3}, Z/4; MoKα 0.71073 Å; / μ 5.730 mm^{-1}, T/173 K. Tmax 0.962, Tmin 1.000; crystal size 0.20x 0.33 x 0.45 mm; No. of measured, independent and observed [I > 2σ(I)] reflections 44368, 6143, 4795 (R_{int} 0.056); R[F^2 > 2σ(F^2)] (all data) 0.0238, wR(F^2) 0.0536, S 0.98; Δρmax, Δρmin 0.64, -0.85 e$Å^{-3}$.

37. A. D. Becke, Density- functional thermochemistry. III. The role of exact exchange, J. Chem. Phys. **(**1993) 5648.

38. C. Lee, W. Yang, R.G. Parr. Development of the Colle-Salvetti correlation-energy formula into a functional of the electron density, Phys. Rev. B 37 (1988) 785.

39. S. Grimme, J. Antony, S. Ehrlich, H. Krieg, A consistent and accurate *ab* initio parameterization of density functional dispersion correction (DFT-D) for the 94 elements H-Pu, J. Chem. Phys. 132 (2010) 154104.

40. P. J. Hay, W. R. Wadt, *Ab* initio effective core potentials for molecular calculations. Potentials for K to Au including the outermost core orbitals, J. Chem. Phys. 82 (1985) 299.

41. T. H. Dunning Jr., P. J. Hay, in Modern Theoretical Chemistry, Ed. H. F. Schaefer III, Vol. 3 (Plenum, New York, 1976) 1.

42. A. E. Reed, L. A. Curtiss, F. Weinhold, Intermolecular interactions from a natural bond orbital, donor-acceptor viewpoint, Chem. Rev. 88 (1988) 899.

43. NBO 5.0. E. D. Glendening, J. K. Badenhoop, A. E. Reed, J. E. Carpenter, J. A. Bohmann, C. M. Morales, F. Weinhold (Theoretical Chemistry Institute, University of Wisconsin, Madison, WI, 2001); http://www.chem.wisc.edu/~nbo5.

44. M. J. Frisch, G. W. Trucks, H. B. Schlegel, G. E. Scuseria, M. A. Robb, J. R. Cheeseman, G. Scalmani, V. Barone, B. Mennucci, G. A. Petersson, H. Nakatsuji, M. Caricato, X. Li, H.P. Hratchian, A. F. Izmaylov, J. Bloino, G. Zheng, J. L. Sonnenberg, M. Hada, M. Ehara, K. Toyota, R. Fukuda, J. Hasegawa, M. Ishida, T. Nakajima, Y. Honda, O. Kitao, H. Nakai, T. Vreven, J.A. Montgomery, Jr., J.E. Peralta, F. Ogliaro, M. Bearpark, J. J. Heyd, E. Brothers, K. N. Kudin, V.N. Staroverov, R. Kobayashi, J. Normand, K. Raghavachari, A. Rendell, J.C. Burant,

S. S. Iyengar, J. Tomasi, M. Cossi, N. Rega, J. M. Millam, M. Klene, J. E. Knox, J.B. Cross, V. Bakken, C. Adamo, J. Jaramillo, R. Gomperts, R. E. Stratmann, O. Yazyev, A. J. Austin, R. Cammi, C. Pomelli, J. W. Ochterski, R. L. 1 Martin, K. Morokuma, V. G. Zakrzewski, G. A. Voth, P. Salvador, J. J. Dannenberg, S. Dapprich, A. D. Daniels, O. Farkas, J. B. Foresman, J. V. Ortiz, J. Cioslowski, D. J. Fox, The Gaussian, Inc., Wallingford CT (2009).

45. S. Ahmad, A. A. Isab, A. R. Al-Arfaj and A. P. Arnold, Synthesis of cyano(selenone)gold(I) complexes and investigation of their scrambling reactions using ^{13}C and ^{15}N NMR spectroscopy, Polyhedron 21 (2002) 2099-2105.

46. S. Ahmad, A. A. Isab, Silver(I) complexes of selenourea (^{13}C and ^{15}N labeled); characterization by ^{13}C, ^{15}N and ^{107}Ag NMR, Inorg. Chem. Commun. 5 (2002) 355-357.

47. A. A. Isab, M. I. M. Wazeer, M. Fettouhi, S. Ahmad, W. Ashraf, Synthesis and Characterization of Mercury(II) Complexes of Selones: X-ray Structure, CP MAS and Solution NMR Studies, Polyhedron 25 (2006) 2629-2636.

48. A. Ahmad, A. A. Isab, Mixed ligand gold(I) complexes with phosphines and selenourea, Transition Met. Chem. 28 (2003) 540–543.

49. M. Fettouhi, M. I. M. Wazeer, S. Ahmad, A. A. Isab, X-ray structure and ^{77}Se, ^{31}P and ^{13}C MAS NMR of the dinuclear complex 1,2-bis(selenourea)-1kSe, 2kSe-1,2-bis(trimethylphosphine)digold(I) chloride, Polyhedron 23 (2004) 1–4.

50. P. G. Jones, C. Thone, Gold Complexes with Selenium Ligands, IV Preparation, Crystal Structures and Reactions of Phosphine(selenourea)gold(I) Complexes, Chem. Ber. 124 (1991) 2725.

51. J. S. Rutherford, C. Calvo, The crystal structure of selenourea, Z. Kristallogr. 128 (1969) 229–258.

52. A. A. A. Sulaiman, M. Altaf, A. A. Isab, A. Alawad, S. Altuwaijri, S. Ahmad, Synthesis, Characterization, and *in vitro* Cytotoxicity of Gold(I) Complexes of 2-(Diphenylphosphanyl)ethylamine and Dithiocarbamates, Z. Anorg. Allg. Chem. 642 (2016) 1454–1459.

661 53. S. Chauhan, K. Singh, K. Kumar, S. C. Neelakantan, G. Kumar, Drug-Amino
662 Acids Interactions in Aqueous Medium: Volumetric, Compressibility and
663 Viscometric Studies, J. Chem. Eng. Data. 61 (2016) 788-796.

664 54. C.C. McIlwain, D.M. Townsend, K.D. Tew, Glutathione S-transferase
665 polymorphisms: cancer incidence and therapy, Oncogene 25 (2006) 1639–1648.

666 55. D.M. Townsend, K.D. Tew, The role of glutathione-S-transferase in anti-cancer
667 drug resistance, Oncogene 22 (2003) 7369–7375.

668 56. T. Shoeib, D.W. Atkinson, B.L. Sharp, Structural analysis of the anti-arthritic drug
669 Auranofin: Its complexes with cysteine, selenocysteine and their fragmentation
670 products, Inorg. Chim. Acta 363 (2010) 184–192.

671